Establishing a New Mechanical Nonlinear Coefficient Q from FT-Rheology: First Investigation of Entangled Linear and Comb Polymer Model Systems

Kyu Hyun[†,‡] **and Manfred Wilhelm***[,‡]

Max-Planck-Institute for Polymer Research, Ackermannweg 10, 55128 Mainz, Germany and Institute for Chemical Technology and Polymer Chemistry, Universität Karlsruhe (TH), Engesserstrasse 18, 76128 Karlsruhe, Germany

Received July 29, 2008; Revised Manuscript Received October 20, 2008

ABSTRACT: The nonlinear response of monodisperse linear and comb polymer melts has been investigated under oscillatory shear with Fourier-transform rheology (FT-rheology). The relative intensity of the third harmonics ($I_{3/1}$), which quantify nonlinearity, was found to depend on the strain amplitude (γ_0) at small and medium strain amplitudes quadratically regardless of the excitation frequency, temperature, and polymer topology. From these results, for the first time, we proposed new nonlinear coefficient Q, which is defined as $Q \equiv I_{3/1}/\gamma_0^2$, and we also defined zero-strain nonlinearity, Q_0, as a constant value at relatively small strain amplitude ($\lim_{\gamma_0 \to 0} Q \equiv Q_0$; e.g., the zero shear viscosity). In the case of the linear polymer melt, the Q value displays a constant value at small and medium strain amplitude. At large strain amplitude, we detect that the value of Q is finally reduced ($Q(\gamma_0)$ is decreasing). The investigated comb polymer shows very different behavior; the value of Q displays an overshoot ($Q(\gamma_0)$ is increasing). The $Q_0(\omega)$ shows time−temperature superposition (TTS) behavior that is very similar to that of the linear viscoelastic properties. Using TTS, we create master curves of $Q_0(\omega)$ over a wide range of frequency. The $Q_0(\omega)$ for linear PS displays a relaxation process of disentanglement of polymer chains such as linear viscoelastic properties. Experimentally, we find that $Q_0(\omega)$ displays very different results for monodisperse linear and comb polymer melts. More specifically, $Q_0(\omega)$ of comb polymers with entangled branches robustly exhibits two relaxation processes that are currently related to the relaxation process of branches and the backbone chain. In this article, for the first time, we proposed this new nonlinear coefficient Q and the zero-strain nonlinearity Q_0 from FT-rheology. This analysis is applied to the investigation of the entangled linear monodisperse polymer and comb polymer melts. In the current stage, we assume that polymer topology has a strong influence on these nonlinear coefficients (Q and Q_0). This coefficient $Q_0(\omega)$ additionally opens up the possibility for quantitative comparisons between experiments and simulations under nonlinear oscillatory shear.

I. Introduction

Large amplitude oscillatory shear (LAOS) is a test method for the characterization of complex fluids because independently varying both strain amplitude (γ_0) and frequency (ω) allows a broad spectrum to be covered.[1,2] Moreover, it is relatively easy to generate LAOS flow because oscillatory shear does not involve any sudden jump in shear rate or strain. There are several methods for analyzing the results from the LAOS test: (1) G' and G'' as a function of strain amplitude,[3] (2) stress shape (stress vs time) or Lissajous pattern (stress vs strain),[2,4−7] (3) Fourier transform,[8,9] and (4) generalized storage and loss modulus when decomposing the nonlinear data.[10] The investigation of $G'(\gamma_0)$ and $G''(\gamma_0)$ under LAOS is the simplest method for classifying complex fluids without obtaining raw stress data. For the LAOS test, however, the stress output is no longer purely a single sinusoidal, and the behavior can no longer solely be described in terms of the storage modulus (G') and the loss modulus (G'') because of higher harmonic contributions.[2] Therefore, G' and G'' at large strain amplitude do not provide full information of distorted stress data. Thus, we need to investigate the stress data more precisely and systematically. Stress shape, FT-rheology, and generalized storage and loss modulus methods, however, can analyze the full information of distorted stress data at a large strain amplitude.

The FT-rheology is the most sensitive method of those discussed above. The FT-rheology converts the stress data of the time domain into frequency dependent spectra. The FT-rheology can quantify very weak signals of higher harmonics. However, the FT-rheology method yields a rather complex interpretation because of multiple harmonics. Among the higher harmonics, the relative intensity of the third harmonic ($I_{3/1} \equiv I(3\omega)/I(\omega)$, where ω is the excitation frequency) is the most important in quantifying nonlinearity. The FT-rheology methodology can be applied to various complex fluids, for example, emulsion,[11] suspension,[12] dilute polymer solution, and concentration polymer solution and polymer melt.[13−18] For example, the FT-rheology was used to distinguish linear from branched polymers.[13−18] Neidhöfer et al.[13] reported that linear and star-branched polystyrene (PS) solutions behaved similarly under linear oscillatory conditions. No difference was observed under nonlinear step-shear, but a significant difference was observed under nonlinear oscillatory shear flow. They examined the relative intensity of the third harmonic ($I_{3/1}$) and third phase angle (Φ_3) as a function of frequency (Deborah number) at a fixed strain amplitude for both linear and star-branched PS solutions and concluded that the third phase angle (Φ_3) is a good indicator for detecting the branched structure. Fleury et al.[14] applied two rheological methods to assess the difference among several linear and branched polyethylenes; one by $I_{3/1}$ as a function of strain amplitude and the other by the relaxation after strong nonlinear deformation. It was found that the FT-rheology could be more sensitive to long chain branch (LCB). Schlatter et al.[15] studied the behavior of nine molten polyethylenes (two linear and seven densely and sparsely branched) over a wider frequency range. They investigated the $I_{3/1}$ and the third phase angle (Φ_3). It was found that FT-rheology is

* Corresponding author: E-mail: wilhelm@polymer.uni-karlsruhe.de.
† Max-Planck-Institute for Polymer Research.
‡ Universität Karlsruhe (TH).

10.1021/ma8017266 CCC: $40.75
Published on Web 12/10/2008

sensitive to the architecture of the polymer regarding the molecular weight and its distribution and the number of branches and their length. Vittorias et al.[16] investigated 15 polyethylene samples with FT-rheology to examine the relative intensity of the third harmonic and the third phase shift. They found the optimal experimental conditions for differentiating linear and branched polyethylenes using FT-rheology under LAOS and observed that the LCB polyethylenes exhibit higher nonlinearity than do linear polyethylenes of similar molecular weight distribution (MWD). With these efforts, FT-rheology under LAOS is now regarded to be a very sensitive method for detecting LCB or for distinguishing polymer topology. However, there has been no systematic research regarding the nonlinearity itself (especially $I_{3/1}$) with well-defined entangled homopolymer (e.g., the influence of excitation frequency, temperature, or molecular weight and so on).

Therefore, in this study, we first present a systematic investigation of the nonlinearity ($I_{3/1}$) from FT-rheology. Second, a new nonlinear coefficient under oscillatory shear for well-defined polymer melts (monodisperse linear PS and comb PS melts) shall be established. Hyun et al.[17,18] focused on $I_{3/1}(\gamma_0)$ under medium amplitude oscillatory shear (MAOS: strain amplitude $\gamma_0 \leq 1$) rather than LAOS (strain amplitude $\gamma_0 \geq 1$). They reported that $I_{3/1}$ is affected by the excitation frequency and temperature, but the slope of $I_{3/1}$ on the log−log plot for linear polymer remained constant, scaled quadratically ($I_{3/1} \propto \gamma_0^2$) at small and medium strain amplitude, and then leveled off regardless of the molecular weight, MWD, and excitation frequency from experimental and simulation results. They also reported that the slope of $I_{3/1}$ for branched polymer is slightly less than 2. In the results presented herein, it was found that $I_{3/1}$ quadratically depends on strain amplitude (γ_0) for both linear and comb polymer melts. From these results, we propose a new nonlinear coefficient Q, which is defined as $Q \equiv I_{3/1}/\gamma_0^2$, and we also define a zero-strain nonlinearity Q_0 as a constant value at a relatively low strain amplitude ($\lim_{\gamma_0 \to 0} Q \equiv Q_0$; e.g., the zero shear viscosity). Oscillatory shear test applies, for example, a sinusoidal strain and analyses the resulting stress toward the storage modulus G' and loss modulus G''. The underlying mathematics is very much like dielectric spectroscopy, where a sinusoidal electric field is applied, and the resulting current is quantified with respect to the dielectric storage ε' and loss ε''. Increasing the electric field leads to detectable optical nonlinearities as quantified via hyperpolarizabilities (e.g., $\chi^{(2)}$ or $\chi^{(3)}$). The hyperpolarizability is a material constant that is independent of the electric field. Please be aware that the concept of the mechanical Q coefficient is analogous to the nonlinear optical coefficient $\chi^{(3)}$ $(-3\omega; \omega, \omega, \omega)$.[19] Therefore, the Q coefficient will not vanish like the nonlinear optical coefficient does not vanish but rather remains constant for zero strain amplitude, respective electric field. Consequently, this coefficient reflects the inherent and normalized nonlinear mechanical properties of the material under investigation.

With these new nonlinear coefficients (Q and Q_0), we systematically investigate nonlinearity from the FT-rheology for well-defined monodisperse linear PS and comb PS melts. We compare linear viscoelastic data (G', G'', tan δ) and nonlinear viscoelastic data (Q_0) as a function of frequency for linear and comb PS. We also compare this new nonlinear coefficient Q as a function of strain amplitude for linear PS ($Q(\gamma_0)$ decreasing) with those for comb PS with entangled branches ($Q(\gamma_0)$ increasing).

II. Experimental Section

a. Materials. Anionically synthesized monodisperse linear and comb PSs were used. For the linear samples the number in the code represents the molecular weight; for example, the molecular weight of PS 330K is 330 kg/mol, and that of PS 100K is 100 kg/mol. Linear comb polymers consist of a linear backbone on which linear chains (called branches) are chemically grafted. The combs were also anionically synthesized and were previously carefully characterized.[20,21] The PS comb series C6 and C7 consist of a linear backbone with weight-average molecular weight of the backbone (M_b) of 275 and 860 kg/mol, respectively, and q of ∼25−30 linear branches of varying molecular weight of the arms (M_a) from 11.7 to 47 kg/mol, that is, from unentangled to well-entangled. For PS, a typical literature value of the entanglement molecular weight (M_e) is 17 kg/mol.[22,23] The sample C622 has unentangled branch chains, but sample C632 and C642 have entangled branch chains. Table 1 lists the main molecular characteristics of all samples used in this work.

Table 1. Molecular Characteristics of the Samples Used

sample	M_b (kg/mol) backbone	M_a (kg/mol) branch	q (branches/ backbone)	M_{total} (kg/mol)	$\langle\tau_G\rangle_w$ (s) at 190 °C[a]	molecular structure
PS 76K	75.9			75.9	0.05	linear
PS 100K	100			100	0.14	linear
PS 220K	214			214	2.66	linear
PS 330K	330			330	12.44	linear
C622-PS	275	11.7	30	624	11.63	comb
C632-PS	275	25.7	25	913	28.59	comb
C642-PS	275	47	29	1630	102.06	comb
C722-PS	860	11.7	28	1190		comb
C732-PS	860	25.7	26	1530		comb
C742-PS	860	47	29	2230		comb

[a] The terminal relaxation time was evaluated from linear moduli data at 190 °C.

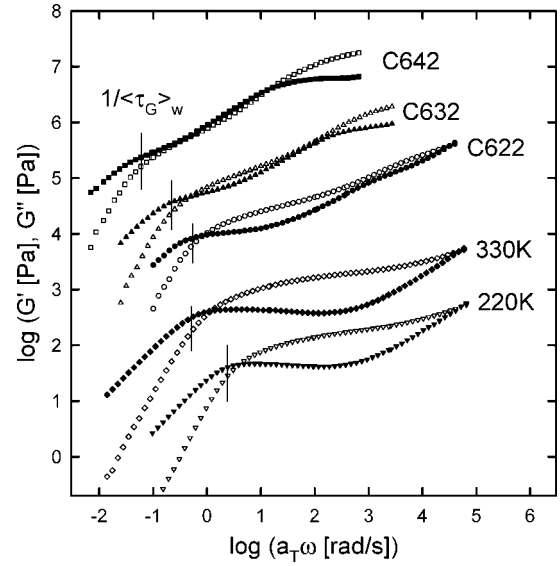

Figure 1. Linear viscoelastic data of linear PS (PS 330K and 220K) and comb PS with equal backbone (M_b = 275 kg/mol) and increasing branch lengths at T_{ref} = 190 °C. The moduli data have been multiplied by 10^{-3} (220K), 10^{-2} (330K), 1 (C622), 10^1 (C632), and 10^2 (C642), respectively, for clarity of presentation. The solid lines indicate $\langle\tau_G\rangle_w^{-1}$.

b. Experimental Methods. Rheological measurements were carried out on a strain-controlled rheometer (ARES, TA Instruments) using a 13 mm parallel-plate fixture with a gap distance of 0.4 mm under a nitrogen environment (99.8% vol) to reduce degradation. Frequency sweep tests (small amplitude oscillatory shear) were carried out at different temperatures, and the master curves were obtained using the time−temperature superposition principle (Figure 1). The data were shifted along the frequency axis, and the horizontal shift factors for all PS samples were fitted with the WLF functions: $\log a_T = [-C_1(T - T_{ref})]/[C_2 + T - T_{ref}]$ with T_{ref} = 190 °C, C_1 = 5.45, and C_2 = 148.23 °C (Figure 2). Strain sweep tests were performed at a fixed frequency and at different

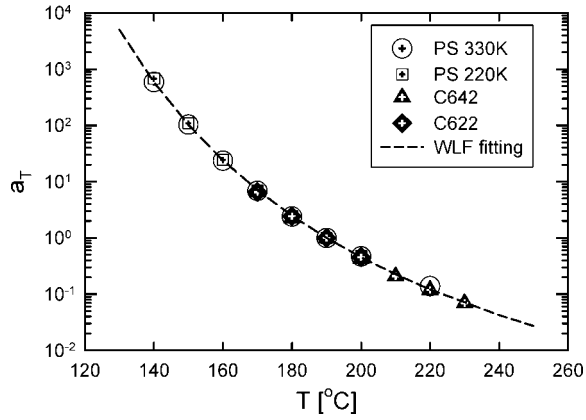

Figure 2. Horizontal shift factor for linear PS and comb PS (symbols). The shift factors were fitted with the WLF function (−−−): $\log a_T = [-C_1(T - T_{ref})]/[C_2 + T - T_{ref}]$ with $T_{ref} = 190$ °C, $C_1 = 5.45$, and $C_2 = 148.23$ °C.

temperatures. For the raw data acquisition, a 16 bit ADC card (PCMCIA-6036E; National Instruments, Austin, TX) with a sampling rate of up to 200 kHz was used. This ADC card was plugged into a laptop computer equipped with laboratory-written LabView (National Instruments) software. The stress data were obtained simultaneously using the ADC card. The stress data as a function of time were analyzed using oversampling[24] and the Fourier transformation technique. From FT analysis, $I_{3/1}$ was plotted as a function of strain amplitude. Noise at low strain amplitude (i.e., γ_0 is below 0.3) does not deteriorate the presented data analysis.[18] At medium strain amplitude, the stress versus time curve still looks sinusoidal to the eye. However, the peak at 3ω (ω: imposed frequency) increases as expected as the strain amplitude increases, even though $I_{3/1}$ is small (usually <0.01). From the high sensitivity FT-rheology method using a high-performance ADC card,[8] these small peaks can be reliably quantified (typical signal-to-noise ratio (S/N) $\approx 10^{-4}$). At relatively large strain amplitude, the distorted stress curve in the time domain and the peaks at higher harmonics in the frequency domain become more obvious.[18]

III. Results and Discussion

a. Linear Viscoelastic Data under Small Amplitude Oscillatory Shear. In Figure 1, we present linear viscoelastic data (G', G'') for linear and comb homopolymer melts of PS. Linear monodisperse PS shows a plateau in G' whose width grows as the molecular weight increases. This plateau is due to the entanglement of polymer chains. Thus, the plateau value of G' is the entanglement plateau modulus. It can be observed that the terminal relaxation time and viscosity increase as a result of the increase in molecular weight (M_w) of the polymer. In the case of comb PS, each macromolecule with specific branch length (M_a) and backbone molecular weight (M_b) has its own signature in the plateau and terminal regions. Thus, there are two rubbery plateaus: one relating to the branches just before they start relaxing and the other relating to the diluted (by the relaxed branches) backbone. Sample C622 has unentangled side branches ($M_a = 11.7 < M_e = 17$ kg/mol, entanglement molecular weight of PS) and exhibits a single rubbery plateau (of the backbone) like linear monodisperse PS. As the branch degree of polymerization increases beyond the entanglement limit (C632 and C642), the onset of a relaxation at higher frequencies corresponding to the branches' disentanglements, in addition to the low frequency terminal relaxation due to the backbone, is observed. The sample C642 displays a power law behavior of the moduli (i.e., G', $G'' \propto \omega^n$, the exponent n is usually in the range of $0 < n < 0.7$) (Figure 1). The value of $n = 1/2$ corresponds to an effective Rouse-like terminal relaxation of the backbone. In terminal regions, the classical behavior $G' \propto \omega^2$ and $G'' \propto \omega$ is observed. Kapnistos et al.[23] explained these results by the dynamic dilution concept.[25−28] As soon as the branches have retracted, they act as effective solvents; as a result, the backbone tube swells, thus decreasing the effective number of entanglements. If the volume fraction of this effective solvent is large enough, then the terminal motion may become that of a chain with few or virtually no entanglements, approaching the behavior of a Rouse chain. The linear viscoelastic terminal relaxation time $\langle \tau_G \rangle_w$ ($= J_e^0 \eta_0$, steady-state compliance $J_e^0 = [G'/(G'')^2]_{\omega \to 0}$ and zero-shear viscosity $\eta_0 = [G''/\omega]_{\omega \to 0}$),[22] evaluated from the linear moduli data, are summarized in Table 1. The terminal relaxation time of linear PS increases with increasing molecular weight. The terminal relaxation time corresponding to the backbone chain of comb PS also increases as a result of the increase in the branches' molecular weight. Because of the backbone chain, the terminal relaxation time is retarded.

b. Nonlinearity under Medium Amplitude Oscillatory Shear. In the framework of the concept of linear response, $I_{3/1}$ is zero because there is by definition no stress distortion. In the nonlinear regime, however, $I_{3/1}$ becomes unequal to zero, and its intensity increases as the strain amplitude increases. $I_{3/1}$ displays a scaling relationship as a function of strain amplitude at small and medium strain amplitude.[17,18]

$$\log(I_3/I_1) = a + b \log \gamma_0 \tag{1}$$

Equation 1 predicts the scaling behavior between $I_{3/1}$ and the strain amplitude with intercept a and slope b. Hyun et al.[18] reported a slope of $I_{3/1}$ (b) of 2 on the basis of the simulation with different constitutive equations (Giesekus, exponential Phan-Thien−Tanner (E-PTT), pom-pom model). This scaling behavior is calculated from the assumption that the sign of the shear stress changes as the sign of shearing changes; therefore, shear stress must be an odd function of the direction of shearing deformations ($\sigma[-\gamma(t), -\dot{\gamma}(t)] = -\sigma[\gamma(t), \dot{\gamma}(t)]$). Thus, the stress curve contains only odd higher harmonic contributions under LAOS flow. (Mathematical equations are found in the literature.)[2,9] The Fourier intensities of the nth harmonics grow with an odd power of the strain amplitude ($I_n \propto \gamma_0^n$, $n = 1, 3, 5...$) in the small and intermediate strain amplitude range.[29] In contrast, the normal stress differences do not change sign if the shear direction is changed. This means that the normal stress differences must be even functions of the direction of shearing deformations ($N_{1,2}[-\gamma(t), -\dot{\gamma}(t)] = N_{1,2}[\gamma(t), \dot{\gamma}(t)]$, $N_{1,2}$ = first and second normal stress differences) and that the intensities of nth harmonics grow with an even power of the strain amplitude ($I_n \propto \gamma_0^n$, $n = 2, 4, 6...$) at small and intermediate strain amplitude.[29] Therefore, the intensity of the third harmonic normalized by the first harmonic scales quadratically on the strain amplitude ($I_{3/1} \equiv I_3/I_1 \propto \gamma_0^3/\gamma_0^1 = \gamma_0^2$) under MAOS. Hyun et al.[17,18] reported the slope of $I_{3/1}$ to be 2 for linear polydisperse polypropylene (PP) and monodisperse PS regardless of the molecular weight, MWD, and imposed excitation frequency. Thus, there are strong indications from both simulation and experiment that the slope of 2 for linear polymers can be general. However, they also reported that the slope of $I_{3/1}$ for branched polymers is <2, even though the pom-pom constitutive model predicts that the slope of $I_{3/1}$ is 2 for H-shaped branched polymer. This discussion is ongoing because of experimental limitation. There is, in principle, the possibility that the slope is 2 at a lower strain amplitude than the investigated range. Because of sensitivity problems, it is very difficult to obtain an exact nonlinearity value at small strain amplitudes (e.g., $\gamma_0 < 0.2$ for polymer melts).[18] Hyun et al.[18] conducted experiments with commercial branched polymer (HDPE, LDPE) but could not find the region of the slope of exactly 2 and measured only one frequency (1 rad/s) for the branched polymer. Here,

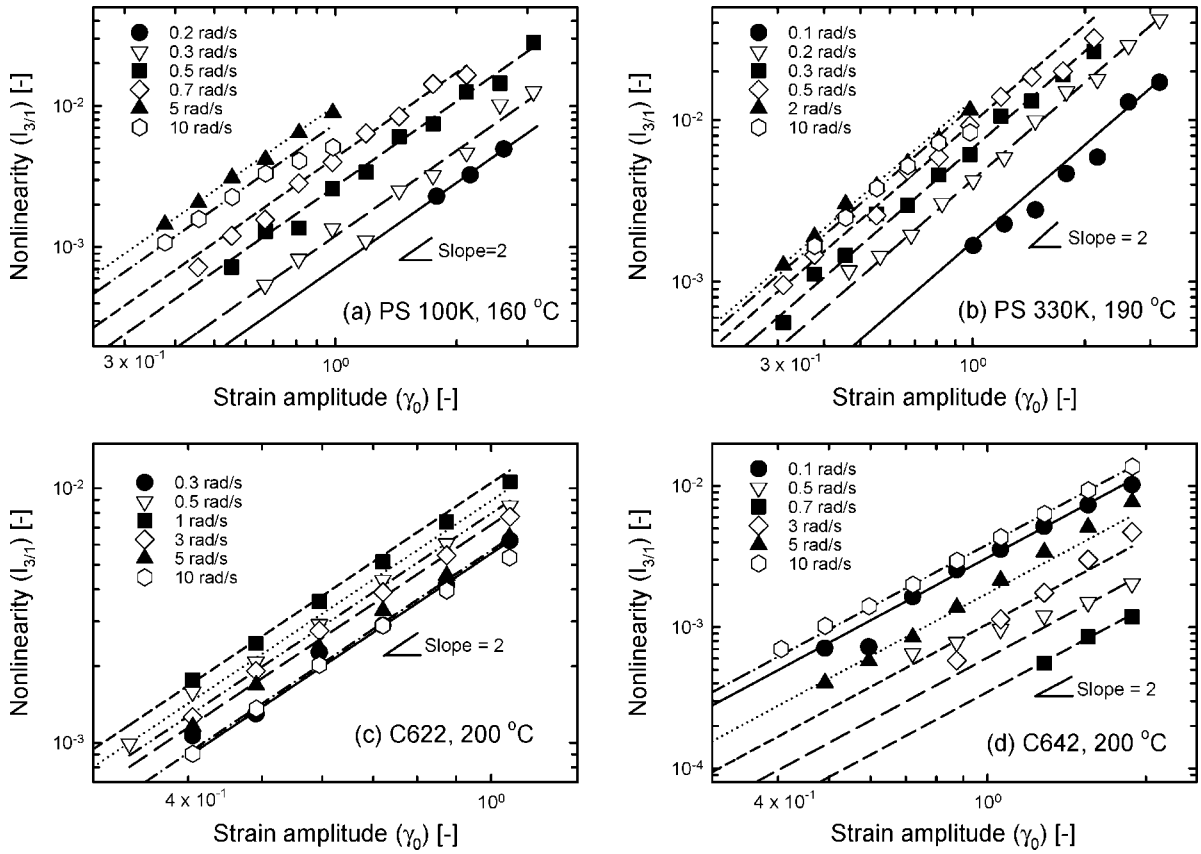

Figure 3. Nonlinearity ($I_{3/1}$) as a function of strain amplitude for linear and comb PS at various frequencies; linear monodisperse (a) PS 100K at 160 °C and (b) PS 330K at 190 °C and comb-polymer (c) C622 at 200 °C and (d) C642 at 200 °C.

however, we investigated $I_{3/1}$ as a function of strain amplitude with well-defined comb polymer melts as well as linear monodisperse polymer at various frequency. We measured $I_{3/1}$ as a function of strain amplitude at various excitation frequency from 0.1 to 10 rad/s. (See Figure 3.) At lower frequencies, $I_{3/1}$ has substantial noise compared with FT-rheology spectra at higher frequencies, and thus data for low frequencies are acquired at higher strain amplitudes. For example, at a frequency of 0.1 or 0.2 rad/s, we measured $I_{3/1}$ up to a strain amplitude of $\gamma_0 \approx 3$. In contrast, at a frequency of 5 or 10 rad/s, we measured $I_{3/1}$ below a strain amplitude of $\gamma_0 \approx 1$. From Figure 3, it is confirmed that the slope of $I_{3/1}$ for linear monodisperse PS is 2 at various frequencies (from $\omega = 0.1$ to 10 rad/s), as was demonstrated by Hyun et al.,[18] and that the slope of $I_{3/1}$ for comb PS is also 2 (C622 and C642; the results of C632, C722, C732, and C742 are not shown here, but they also show the slope to be two), as predicted by the pom-pom model.[18]

c. New Nonlinear Coefficient Q and Zero-Strain Nonlinearity Q_0. From the above results, it is deduced that the nonlinearity quadratically depends on the strain amplitude. Thus, we propose a new nonlinear coefficient, Q, which is defined as

$$Q \equiv I_{3/1}/\gamma_0^2 \tag{2}$$

For this definition, we use the absolute strain amplitude value, not the percent strain amplitude. This new nonlinear coefficient (Q) from FT-rheology is defined using the relationship between stress and deformation like other rheological properties from the steady shear test, for example, viscosity ($\eta \equiv \sigma_{12}/\dot{\gamma}$, where σ_{12} is shear stress and $\dot{\gamma}$ is shear rate), first normal stress coefficient ($\Psi_1 \equiv N_1/\dot{\gamma}^2$, where N_1 is the first normal stress), and second normal stress coefficient ($\Psi_2 \equiv N_2/\dot{\gamma}^2$, where N_2 is the second normal stress). These coefficients often approach constant values at low shear rates; these are called the zero-shear values, η_0, $\Psi_{1,0}$, and $\Psi_{2,0}$.[30] We also defined the nonlinear zero-strain value, Q_0, like the zero shear viscosity as a constant value at relatively low strain amplitude

$$\lim_{\gamma_0 \to 0} Q \equiv Q_0 \tag{3}$$

Using Q_0, we can quantify the inherent or intrinsic nonlinearity as a function of frequency without strain amplitude, as will be later discussed in more detail. Please be aware that zero-strain does not mean that the strain amplitude is actually zero but that the strain amplitude approaches low strain amplitude when the coefficient Q displays constant value. (See Appendix A.) First, using eq 2, we calculated Q values from $I_{3/1}$ and the strain amplitude (γ_0). The coefficient Q was plotted as a function of strain amplitude (see Figure 4). From Figure 4, we observed that the coefficient Q approaches a constant value (zero-strain nonlinearity, Q_0) at small strain amplitude. (This critical strain amplitude is frequency dependent.) The Q value displays scattering around a constant value (Q_0). This is due to $I_{3/1}$ being very low ($3 \times 10^{-4} < I_{3/1} < 10^{-2}$) in the MAOS region (Figure 4). Because the Q_0 is evaluated from several data points (5−10), we are still able to obtain a very reliable Q_0 value. Therefore, it is evident that Q has a constant value (Q_0) at relatively small strain amplitude and otherwise Q is a function of strain amplitude. In particular, we observed that Q is reduced with increasing strain amplitude for linear PS and comb PS with unentangled branches (C622) (Figure 4a,b,c), Q displays overshoot for comb PS with entangled branches (C642) (Figure 4d), and Q has different Q_0 values depending on the imposed frequencies. Before investigating $Q(\gamma_0)$ behavior as a function of strain amplitude under LAOS, we first investigated the effect of excitation frequency on the nonlinearity. From this zero-strain nonlinearity, Q_0, the effect of frequency on the nonlinearity without strain amplitude can be investigated. In the next section,

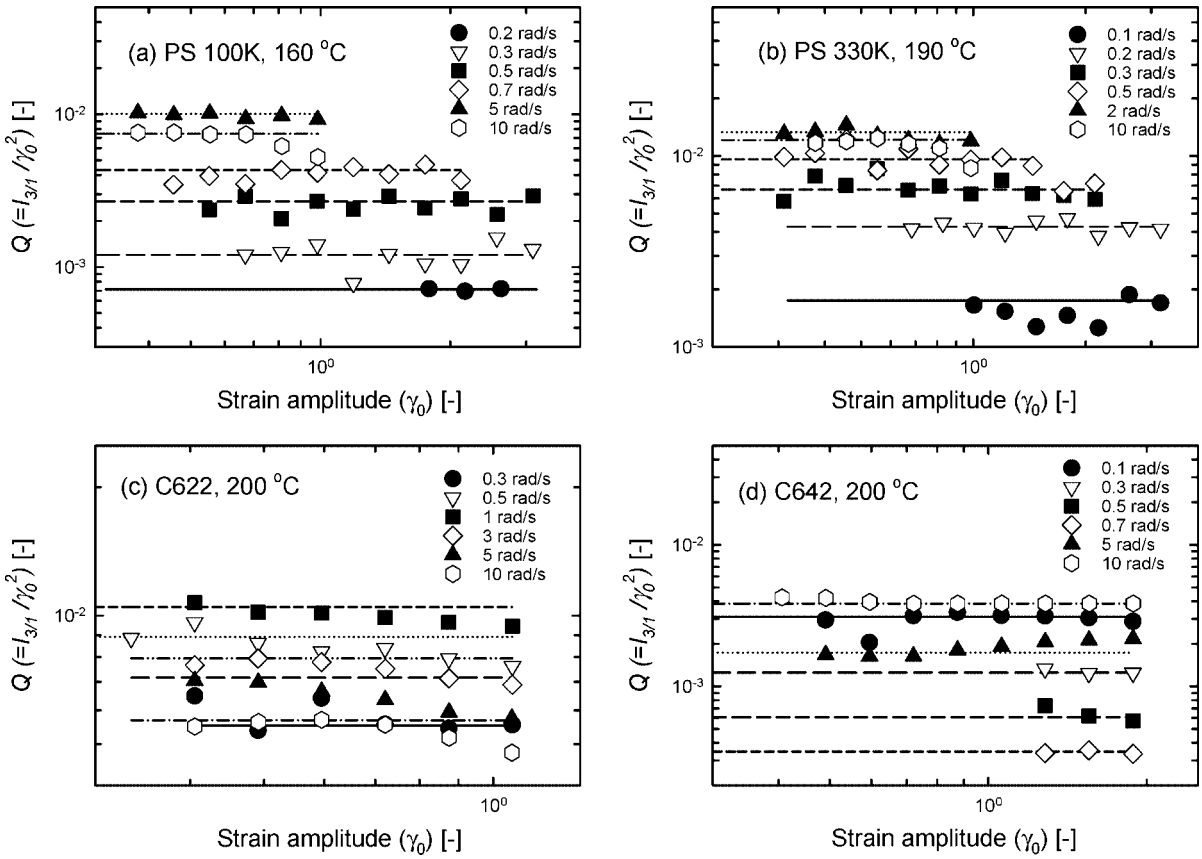

Figure 4. Q coefficient as a function of strain amplitude evaluated from the nonlinearity ($I_{3/1}$) data (a) PS 100K at 160 °C, (b) PS 330K at 190 °C, (c) C622 at 200 °C, and (d) C642 at 200 °C.

the zero-strain nonlinearity, Q_0, as a function of frequency for the linear PS series and comb PS series is investigated.

1. Zero-Strain Nonlinearity, Q_0. In Figure 5, the linear viscoelastic data (G', G'') under SAOS and nonlinear viscoelastic data (Q_0) under MAOS of linear monodisperse PS series with different M_w are plotted as a function of frequency at different temperatures 147 (PS 76K), 160 (PS 100K), 175 (PS 220K), and 190 °C (PS 330K). At these temperatures, each linear PS shows crossover frequency (ω_c) in the linear viscoelastic data (G', G''). As other researchers[13,18] have already pointed out, $I_{3/1}$ displays a maximum around De ($\equiv \omega/\omega_c$) = 1 in case a constant strain amplitude is applied. Thus, these temperatures were selected for obtaining a maximum Q_0. The zero-strain nonlinearity, Q_0, is obtained from the Q coefficient at various frequencies from $\omega = 0.1$ to 10 rad/s. At frequencies of >10 rad/s, edge fracture or instability, even in the medium strain amplitude region ($0.2 \leq \gamma_0 \leq 1$), is a possibility. This affects the nonlinearity, $I_{3/1}$. Chen et al.[31] have investigated the waveform of PS melts at a strain amplitude $\gamma_0 = 4$ and a frequency $\omega/2\pi = 10$ Hz and have observed a rapid decay, followed by shape change of the stress signals. Thus, Q_0 is obtained carefully at frequencies of $\omega < 10$ rad/s. From Figure 5a, the $Q_0(\omega)$ of PS 76K displays a sharp maximum around the terminal relaxation time (Table 1). As molecular weight (M_w) increases, the Q_0 exhibits a plateau behavior (Figure 5c,d for PS 220K and PS 330K, respectively) like the plateau modulus of the storage modulus. A terminal tail follows a maximum in $Q_0(\omega)$. It is evident that Q_0 reflects the relaxation process of the disentanglement of polymer chains like the linear viscoelastic properties. However, to investigate the effect of molecular weight on the Q_0 systematically, a master curve of Q_0 at the same temperature as that of the linear viscoelastic data must be created. We measured the $Q_0(\omega)$ of PS 330K (linear PS) and C622 (comb PS) at various temperatures (Figure 6a,c); then, the $Q_0(\omega)$ were shifted along the frequency axis (Figure 6b,d) at a reference temperature $T_{ref} = 190$ °C. In Figure 7, the horizontal shift factors obtained from nonlinear data (Q_0) are compared with the WLF function from linear viscoelastic data: $\log a_T = [-C_1(T - T_{ref})]/[C_2 + T - T_{ref}]$ with $T_{ref} = 190$ °C, $C_1 = 5.45$, and $C_2 = 148.23$ °C. From this, it is concluded that the time−temperature superposition (TTS) principle is also valid for the nonlinear coefficient, Q_0.[32]The shift factor also applies in the case of comb PS. As previously mentioned, nonlinear viscoelastic coefficient, Q_0 has a larger scatter than the linear viscoelastic data. Therefore, the master curves of nonlinear viscoelastic data (Q_0) are created using the shift factor from the linear viscoelastic data. In Figure 8, the linear and nonlinear viscoelastic master curves of linear monodisperse PS series are plotted as a function of frequency at $T_{ref} = 190$ °C. The terminal relaxation time for each sample with different M_w is plotted as a vertical line in Figure 8. In Figure 8, the Q_0 of PS 76K and PS 100K show the sharp peak that appears at frequencies very close to $1/\langle\tau_G\rangle_w$. However, for the linear PS with the higher molecular weight (PS 220K and 330K), the Q_0 exhibits a broad peak (which almost looks like a plateau). The maximum Q_0 slightly increases with increasing molecular weight (Figure 9). The maximum Q_0 is followed by the terminal tail at frequencies less than $1/\langle\tau_G\rangle_w$. The Q_0 becomes proportional to ω^n (the exponent $n \approx 2$) at low frequencies, $\omega < \omega_{peak}$ ($\approx 1/\langle\tau_G\rangle_w$). Pearson and Rochefort[33] calculated higher-order terms from the Doi−Edwards model. We calculated Q from these high-order terms and obtained a quadratic scaling ($Q_0 \propto \omega^2$) at low-frequency limit. (See Appendix B.) From experimental results, it is difficult to investigate the quadratic scaling ($Q_0 \propto \omega^2$). There are two problems in obtaining the coefficient Q_0 for the low frequency limits: one is the extremely low torque value and the other is the low nonlinearity ($Q_0 < 10^{-3}$). The terminal zone characterized by these ω dependencies shifts to the lower

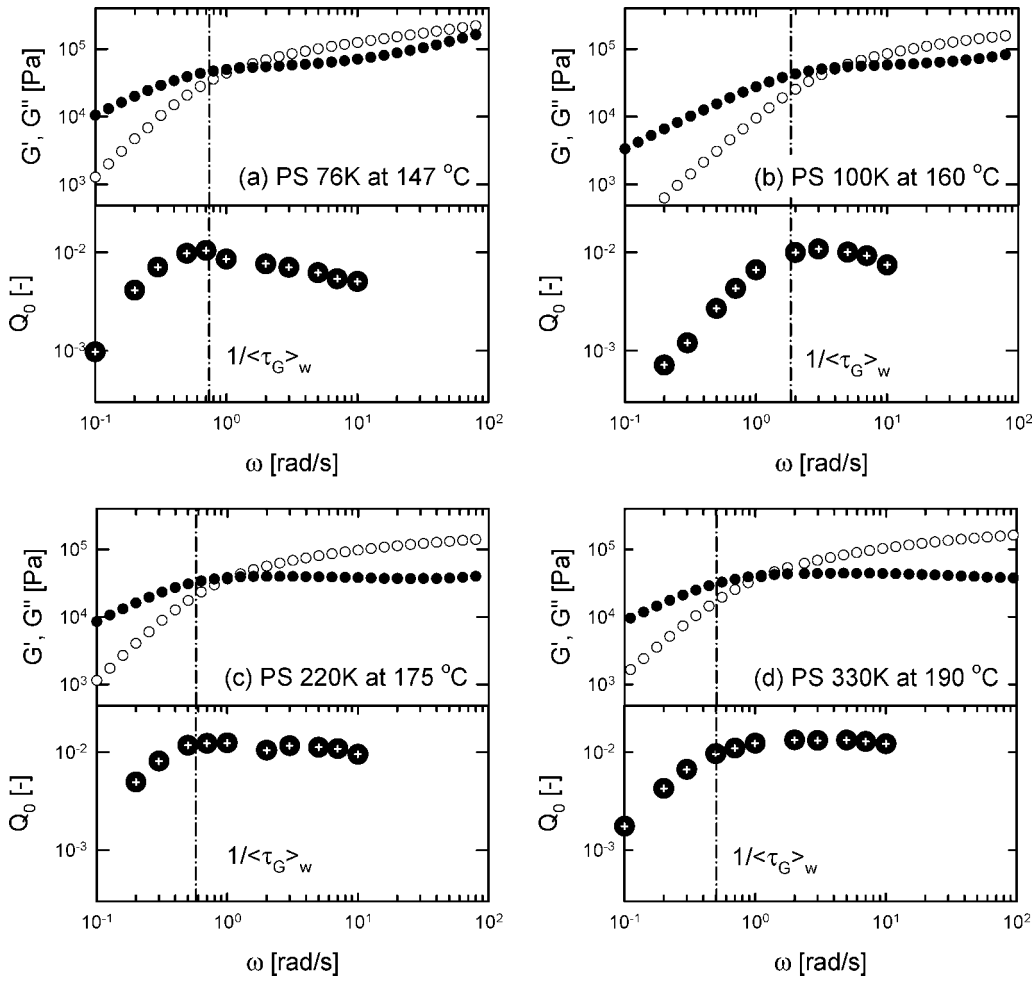

Figure 5. Linear viscoelastic data (G', G'') under small amplitude oscillatory shear (SAOS) and nonlinear viscoelastic data (zero-strain nonlinearity, Q_0) under medium amplitude oscillatory shear (MAOS) as a function of frequency for linear PS (a) PS 76K at 147 °C, (b) PS 100K at 160 °C, (c) PS 220K at 175 °C, and (d) PS 330K at 190 °C. The dashed−dotted lines indicate $\langle \tau_G \rangle_w^{-1}$.

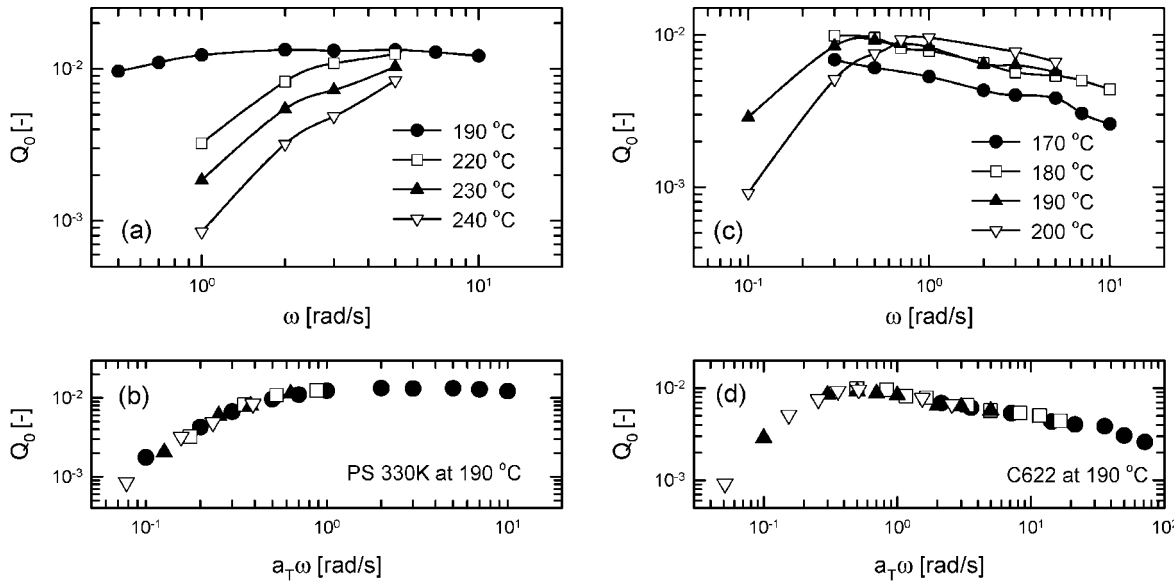

Figure 6. $Q_0(\omega)$ at different temperature. (a) Q_0 for PS 330K at 190, 220, 230, and 240 °C, (b) Q_0 for C622 at 170, 180, 190, and 200 °C, and the master curve of Q_0 at T_{ref} = 190 °C (c) PS 330K and (d) C622.

frequencies with increasing M_w. From these results, it is evident that the zero-strain nonlinearity $Q_0(\omega)$ reflects the relaxation process of the polymer chain motion including terminal behavior and the plateau value via physical entanglements. From this, it is inferred that $Q_0(\omega)$ can also reflect the relaxation process of polymers with different topologies and, conversely, polymer topology should additionally affect the nonlinear coefficient $Q_0(\omega)$.

This statement should motivate our investigation of linear and comb polymers. Therefore, we investigated well-defined

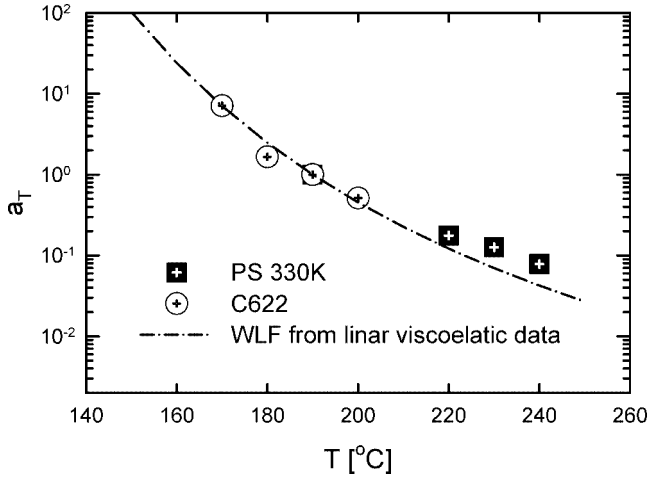

Figure 7. Comparison of the shift factor from nonlinear viscoelastic data (symbols) with the WLF fitting function (———) from linear viscoelastic data.

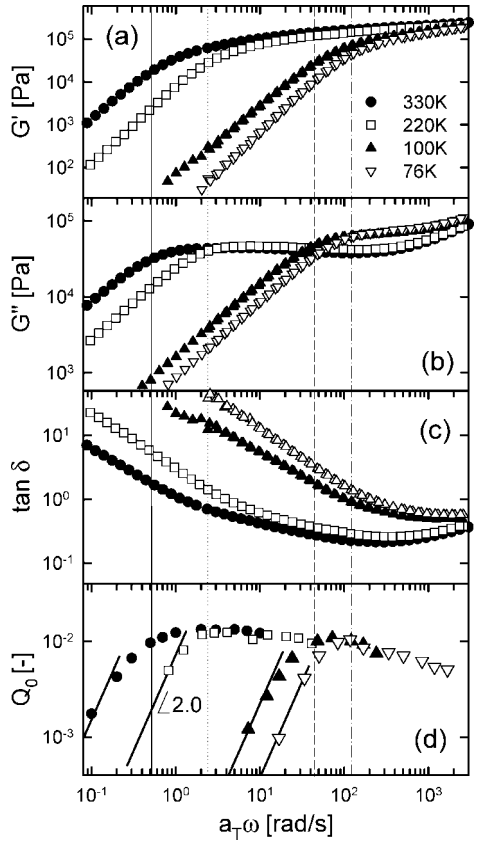

Figure 8. Master curve of linear viscoelastic and nonlinear viscoelastic data for monodisperse linear PS (76K, 100K, 220K, and 330K) at T_{ref} = 190 °C. (a) Storage modulus (G'), (b) loss modulus (G''), (c) tan δ under SAOS, and (d) zero-strain nonlinearity Q_0 under MAOS.

comb PS topologies. The linear (G', G'', tan δ) and nonlinear (Q_0) viscoelastic data of comb PS series are plotted in Figure 10 (Figure 10a,b for C622 and C642, respectively). At lower frequencies, both C622 and C642 show terminal behavior like monodisperse linear PS ($Q_0 \propto \omega^2$). For the sample C622 with an unentangled side branch chain ($M_a = 11.7 < M_e = 17$ kg/mol), $Q_0(\omega)$ shows only one maximum like linear PS. The unentangled side branch chain does not significantly decrease the relaxation process of the backbone chain. In contrast, the Q_0 of the C642 with entangled branch chain ($M_a = 47 > M_e = 17$ kg/mol) displays two relaxation processes: one corresponding

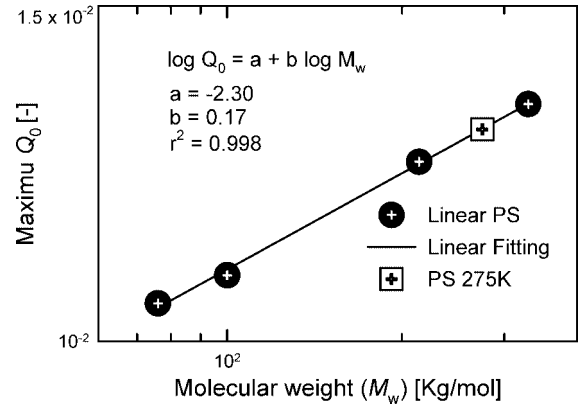

Figure 9. Maximum $Q_0(\omega)$ of each linear PS with different molecular weight from Figure 8. The solid line indicates the relationship between maximum Q_0 and molecular weight. From this equation, the maximum Q_0 of PS 275K corresponding to the molecular weight of the C6 comb-PS series' backbone chain is evaluated.

to the branches' disentanglements and the other due to the backbone chain. Between the two distinct relaxation processes, the $Q_0(\omega)$ decreases and displays a local minimum of Q_0. This frequency region corresponds to the linear viscoelastic data where a power law behavior of the moduli (i.e., G', $G'' \propto \omega^n$, exponent $n \approx {}^1/_2$ (an effective Rouse-like terminal relaxation of the backbone)) and the low-frequency plateau (tan δ) (Figure 10b) exist.[23] The behavior in the region between the two vertical dashed lines in Figure 10b can be explained by the dynamic dilution concept, as previously explained. As soon as the branches have fully relaxed by retraction, they act as effective solvents; as a result, the backbone tube swells, thus decreasing the effective number of its entanglements. If the volume fraction of this effective solvent is large enough, then the terminal motion may become that of a chain with few or virtually no entanglements, which approaches the behavior of a Rouse chain.[23] Thus in the zero-strain nonlinearity, Q_0, being very sensitive to the entanglements of polymers, displays a detectable local minimum within this frequency region. For C642, we observed a second terminal tail ($Q_0 \propto \omega^2$) corresponding to the relaxation process of the branches' disentanglement at frequencies higher than ω_{min} (the frequency of minimum Q_0). This means that $Q_0(\omega)$ can reflect the relaxation process of polymer chains, as was already detected for linear PS. In particular, the comb PS with entangled linear branches, $Q_0(\omega)$ displays two peaks: one at higher frequencies corresponding to the branches' disentanglements and the other at lower frequencies due to the backbone. This separation of $Q_0(\omega)$ is very well explained by the hierarchical relaxation process of branched polymer.[25] In Figure 11, the linear (G', G'', tan δ) and nonlinear (Q_0) viscoelastic data of the comb-PS series with different degree of branches (C622, C632, and C642) are plotted at T_{ref} = 190 °C. As the molecular weight of the side arms (M_a) increases, the terminal tail of the backbone shifts to lower frequencies. As the branch chain length increases, the terminal relaxation time of the backbone is retarded. This behavior differs with that exhibited by linear PS, where the maximum of $Q_0(\omega)$ slightly increases with increasing molecular weight (Figure 9). The maximum of $Q_0(\omega)$ corresponds to the relaxation of the backbone chain ($Q_{0,b}$). The maximum value decreases as the total molecular weight or branch molecular weight increases. This can be explained by the dynamic tube dilution concept. As the backbone volume fraction (ϕ_b) in the entire comb molecule decreases, the dilution process by branch chains becomes stronger, and thus the maximum Q_0 also decreases. In Table 2, the maximum $Q_0(\omega)$ values corresponding to the relaxation of the backbone ($Q_{0,b}$) of comb PS of different branch chain length are evaluated. To

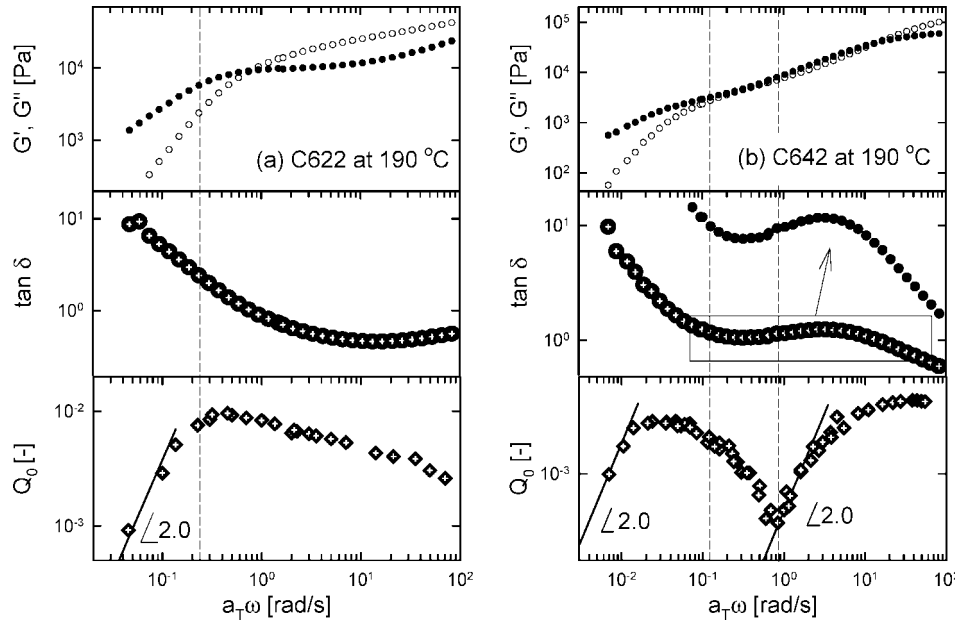

Figure 10. Master curve of linear viscoelastic and nonlinear viscoelastic data for comb PS (a) C622 and (b) C642 at $T_{ref} = 190$ °C.

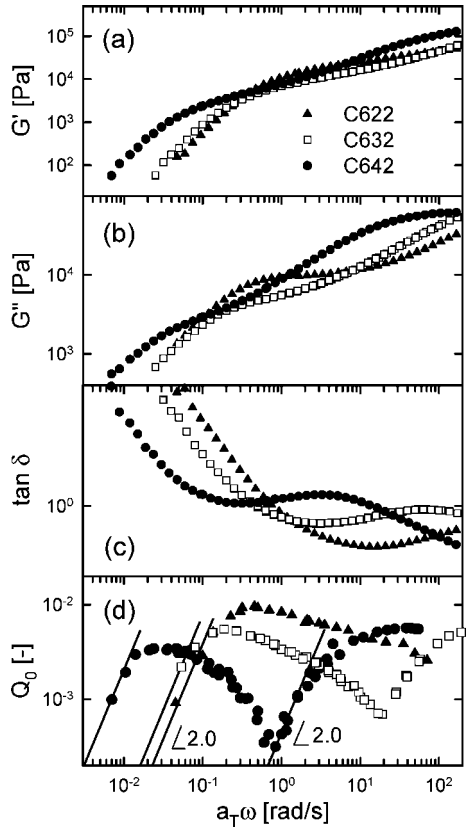

Figure 11. Master curve of the linear viscoelastic and nonlinear viscoelastic data for comb PS (C622, C632, and C642) at $T_{ref} = 190$ °C. (a) Storage modulus (G'), (b) loss modulus (G''), (c) tan δ under SAOS, and (d) zero-strain nonlinearity Q_0 under MAOS.

compare linear and comb PS, the $Q_0(\omega)$ of linear and comb PS are plotted at $T_{ref} = 190$ °C in Figure 12a. The $Q_0(\omega)$ is shifted using relaxation times for each sample in Figure 12b. As a result, the terminal tails of all samples (linear and comb polymer) almost overlap. In Figure 12a,b, it is confirmed that the maximum Q_0 corresponding to the relaxation process of the backbone chain ($Q_{0,b}$) decreases as the backbone chain's volume fraction decreases for the samples investigated here. The comb

Table 2. Maximum Q_0 Values Corresponding to Backbone Chain Relaxation

sample	$Q_{0,b}$ ($\times 10^2$)	ϕ_b (M_b/M_{total}) volume fraction of backbone	$Q_{0,b}/Q_{0,b,275K}$	molecular structure
PS 275K[a]	1.292		1	linear
C622-PS	0.924	0.44	0.715	comb
C632-PS	0.551	0.30	0.427	comb
C642-PS	0.344	0.17	0.266	comb

[a] PS 275K is calculated from Figure 9 using a relation between Q_0 and molecular weight.

PS with unentangled branch chains (C622) shows a relaxation shape similar to that of linear PS; however, the $Q_{0,b}$ is lower than that for other linear PS. This means that the nonlinearity $Q_0(\omega)$ is highly related to the effective entanglements and corresponding volume fraction. In Figure 12b, the slope of $Q_0(\omega)$ after the first terminal tail corresponding to the backbone chain increases as the branch length increases ($Q_0 \propto \omega^{-0.22}$ for C622; $\omega^{-0.4}$ for C632; and $\omega^{-0.5}$ for C642 in Figure 12b). This tendency toward broader peaks is in accord with the results of dielectric behavior, which reflects the global polymer chain motion, of polyisoprene (PI) in an oligo(butadiene).[34] In the dilute regime (nonentangled PI), the dielectric mode distribution is narrow and insensitive to the concentration of linear PI (c_{PI}) and then broadens with increasing c_{PI} and again becomes insensitive to c_{PI} above the overlapping concentration (entangled PI).[34] In the case of our comb PS series (C622, C632, and C642), the volume fraction of the backbone chain decreases as the branch chain length increases (Table 2). As far as the dynamic tube dilution concept is concerned, the already fully relaxed branched polymer chain acts as an effective solvent for the unrelaxed backbone chain. The increasing branch chain length has a similar effect of decreasing the concentration of the backbone chain in solvent. Therefore, the Q_0 frequency distribution after the first terminal tail becomes narrower ($Q_0 \propto \omega^{-0.22}$ for C622; $\omega^{-0.4}$ for C632; and $\omega^{-0.5}$ for C642) as the branch chain length increases. From these observations, the decreasing of maximum Q_0 and the narrowing of Q_0 correspond to the backbone chain relaxation with increasing branch chain length and the two relaxation processes for the comb polymer with entangled side chains. Therefore, we conclude that it is evident that the $Q_0(\omega)$ reflects the relaxation process of disentanglement

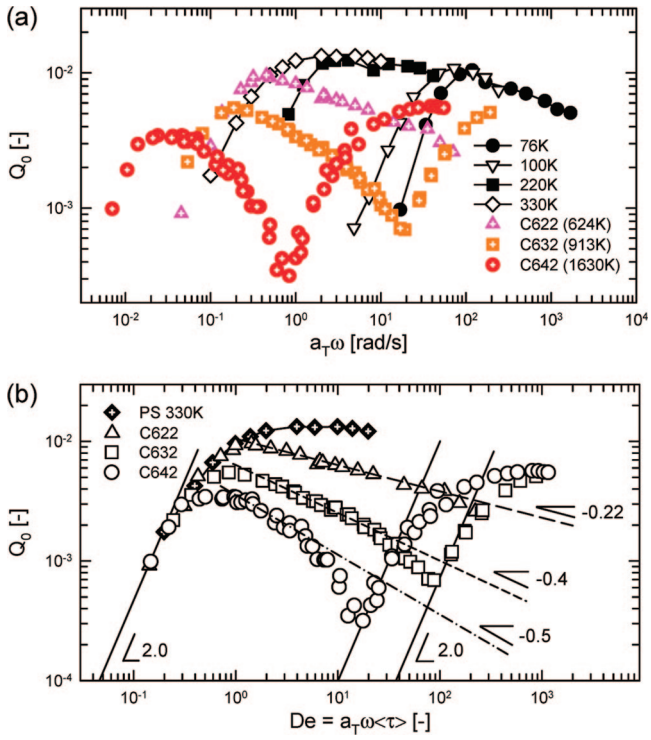

Figure 12. (a) Q_0 of linear PS (76K, 100K, 220K, and 330K) and comb PS (C622, C632, and C642) at $T_{ref} = 190$ °C. (b) For a clear comparison, Q_0 is plotted against the De number ($= a_T\omega<\tau>$) of linear PS 330K and comb PS (C622, C632, and C642) at $T_{ref} = 190$ °C.

of polymer chain including reptation, contour length fluctuation, and constraint release.

Kapnistos et al.[23] reported that among linear viscoelastic data (G', G'', tan δ), the phase angle (tan δ) is a sensitive indicator of the appearance of the two relaxation processes. However, by a comparison of the frequency dependence of the linear viscoelastic data (tan δ) and the zero-strain nonlinearity Q_0, it is conclusive that the $Q_0(\omega)$ is a more sensitive indicator of the appearance of the two relaxation processes than are the linear viscoelastic data.

2. $Q(\gamma_0)$ under Large Amplitude Oscillatory Shear. In this section, the behavior of the $Q(\gamma_0)$ coefficient with increasing strain amplitude is investigated at a fixed frequency. For monodisperse linear PS, a decrease in Q as strain amplitude increases ($Q(\gamma_0)$ decreasing) is observed (Figure 4a,b) at various frequencies like shear thinning from shear rate experiments. At higher frequencies, the decrease in $Q(\gamma_0)$ starts at lower strain amplitude compared with the decrease at lower frequencies. In Figure 13, the Q values of PS 100K and PS 330K at frequency $\omega = 10$ rad/s decrease below strain amplitude $\gamma_0 = 1$ in contrast with those at frequency $\omega = 0.2$ rad/s, which still show a constant value at $\gamma_0 = 1$. Usually, the degree of deformation under oscillatory shear is determined by the frequency (ω) and strain amplitude (γ_0). Thus, at higher frequency, the decrease in $Q(\gamma_0)$ starts at a lower strain amplitude than that at lower frequency. To investigate the decrease in $Q(\gamma_0)$ in more detail, Q from low strain amplitude ($\gamma_0 \approx 0.3$) to large strain amplitude ($\gamma_0 \approx 7$) was measured for PS 100K at $\omega = 4.25$ rad/s, 160 °C. The normalized nonlinearity Q/Q_0 as a function of strain amplitude is compared with the normalized complex modulus $|G^*|/|G^*_0|$. ($|G^*_0|$ is a linear complex modulus under SAOS at a fixed frequency; see Figure 14a.) In Figure 14a, both $|G^*|/|G^*_0|$ and Q/Q_0 decrease as a function of strain amplitude, and the degree of decreasing is similar. For a comb PS with unentangled branches (C622), a decrease of $Q(\gamma_0)$ like that in a linear monodisperse PS is observed at various frequency. This can be seen in Figure 4c. In Figure 14b, both $|G^*|/|G^*_0|$ and Q/Q_0 of

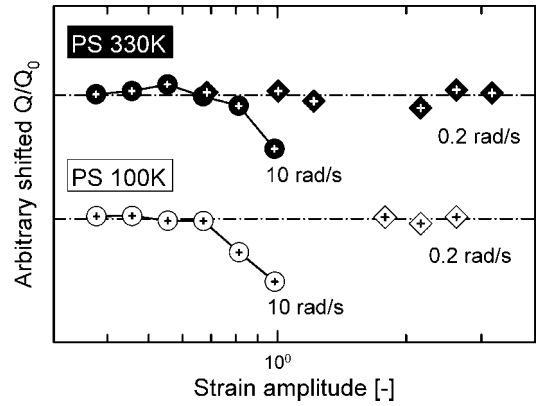

Figure 13. Q/Q_0 of linear PS (100K and 330K) as a function of strain amplitude at two frequencies (10 and 0.2 rad/s). At a relatively high frequency of 10 rad/s, the strain softening in Q/Q_0 starts at a lower strain amplitude ($\gamma_0 < 1$). However, at a low frequency 0.2 rad/s, the Q/Q_0 still displays a constant value above $\gamma_0 \approx 1$.

C622 are plotted from low strain amplitude ($\gamma_0 \approx 0.3$) to large strain amplitude ($\gamma_0 \approx 8$) at $\omega = 1$ rad/s and $T = 200$ °C. It is evident that the Q coefficient is reduced with increasing strain amplitude ($Q(\gamma_0)$ is decreasing) for C622. As previously mentioned, because C622 has unentangled side branch chains, the general nonlinear behavior ($Q(\gamma_0)$ is decreasing and the relaxation process from $Q_0(\omega)$) of comb PS C622 is similar to that of linear PS. On the contrary, the Q of comb PS with entangled side branches (C642) increases as the strain amplitude increase ($Q(\gamma_0)$ is increasing) at $\omega = 5$ rad/s in Figure 4d. A more detailed analysis of $Q(\gamma_0)$ of C642 under LAOS at various frequency was performed. The Q of C642 is plotted as a function of strain amplitude at $T = 190$ °C in Figure 15. At $\omega = 1$ rad/s, a strong overshoot of Q ($Q(\gamma_0)$ is increasing) is observed. As the frequency increases, this overshoot becomes weaker until it finally disappears at $\omega = 5$ rad/s. The nonlinearity $Q_0(\omega)$ has a local minimum around 1 rad/s. (See Figure 12.) Even though the nonlinearity, Q, at a frequency of 1 rad/s is very small (the local minimum point), the normalized nonlinearity (Q/Q_0) shows a stronger overshoot than at all other frequencies (Figure 15b). At $\omega = 5$ rad/s, the normalized nonlinearity (Q/Q_0) shows a decrease in $Q(\gamma_0)$ instead of an increase in $Q(\gamma_0)$ (not shown here; at $\omega = 0.1$ rad/s, the Q/Q_0 decrease as a function of the strain amplitude). From the above results, C622 with unentangled branches shows only a decrease in $Q(\gamma_0)$ at various frequencies; on the contrary, C642 with entangled branches shows $Q(\gamma_0)$ increasing behavior at specific frequency regions. It is well known that the strain hardening behavior in elongational flow is highly related to the branched polymer chain. The increase in Q reflects the effect of the branched polymer chain. Thus, the $Q(\gamma_0)$ coefficient is affected by the polymer topology. However, we still do not fully understand the underlying nonlinear physics that predicts the $Q(\gamma_0)$ behavior. Therefore, further theoretical and experimental studies are needed to understand the Q behavior as a function of the strain amplitude of entangled polymer with different topology.

For the comb PS with entangled branch chains, the increase in $Q(\gamma_0)$ occurs at specific frequencies. This means that frequency is also very important for investigating MAOS and LAOS flow, and the Q coefficient has a different value as frequency changes. The increase in Q as a function of strain amplitude seems to be promising parameter for detecting long chain branching in commercial branched polymers, for example, LCB-PE.

IV. Conclusions

The nonlinear behavior of monodisperse linear and comb PS melts under oscillatory shear (MAOS and LAOS) were studied

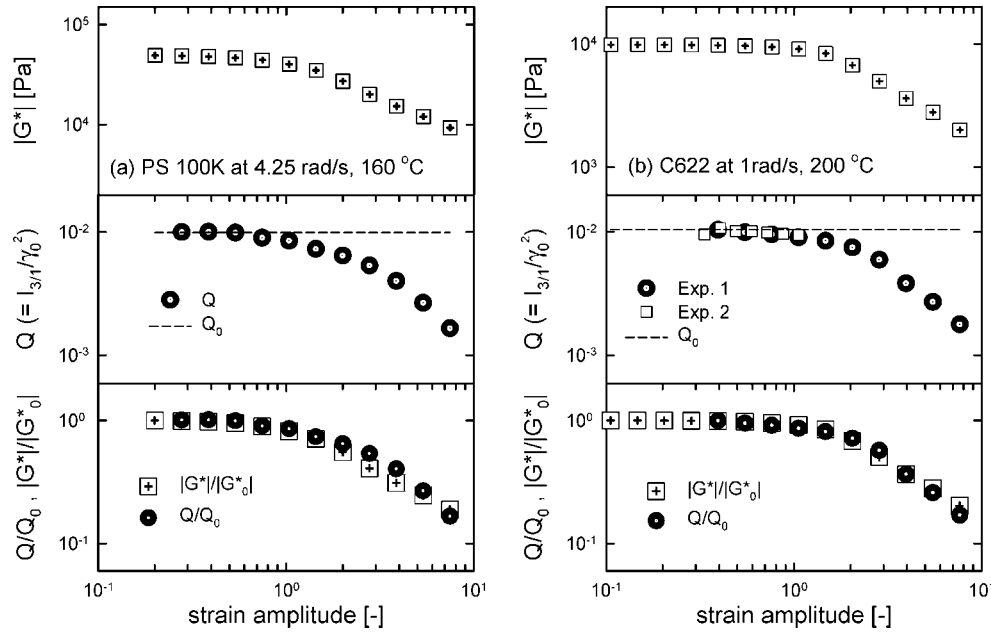

Figure 14. $|G^*|$ and Q as a function of strain amplitude from medium strain amplitude ($\gamma_0 \approx 0.25$) to large strain amplitude ($\gamma_0 \approx 7$) and the comparison of normalized $|G^*|/|G^*_0|$ with normalized Q/Q_0. (a) Monodisperse linear PS (100K) at $\omega = 4.25$ rad/s and $T = 160$ °C and (b) comb PS with unentangled branch (C622) at $\omega = 1$ rad/s and $T = 200$ °C. Both linear PS and comb PS with unentangled branch exhibit strain softening as strain amplitude increase.

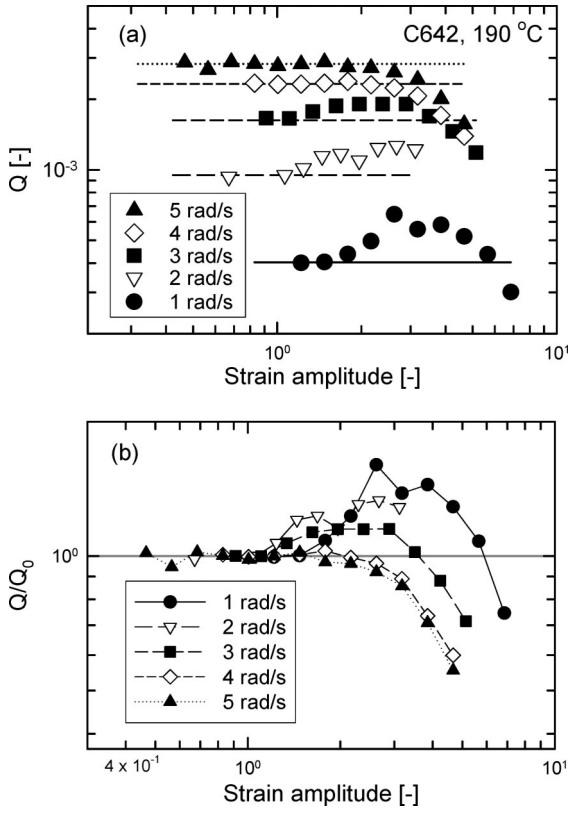

Figure 15. (a) Q and (b) normalized Q/Q_0 as a function of strain amplitude at various frequencies (1, 2, 3, 4, and 5 rad/s) for comb PS with entangled branch chains (C642).

with FT-rheology. The relative intensity ($I_{3/1}$) of the third harmonics for both linear and comb PS were found to depend on the strain amplitude at low and medium strain amplitudes quadratically. From these results, we proposed a new nonlinear coefficient, Q, which is defined as $Q = I_{3/1}/\gamma_0^2$, and we also defined zero-strain nonlinearity, Q_0, as a constant value at relatively low strain amplitude ($\lim_{\gamma_0 \to 0} Q \equiv Q_0$). The Q_0 under MAOS of monodisperse linear PS as a function of frequency displays a relaxation process with one peak value and a terminal behavior ($Q_0 \propto \omega^2$) at low frequencies. As the molecular weight increases, the terminal behavior shifts to lower frequencies like the linear viscoelastic properties, and the peak becomes broader to the point of almost being a plateau. In the case of comb PS with unentangled branch chains (C622), the $Q_0(\omega)$ displays a similar shape as a function of frequency (one maximum value and terminal tail ($Q_0 \propto \omega^2$)). In contrast with linear PS, however, the maximum Q_0 is lower than that for other linear monodisperse PS. This could be due to the dynamic tube dilution induced by the branch chains. In particular, for the comb PS with entangled branch chains (C632 and C642), $Q_0(\omega)$ has two peak values: one corresponds to the branches' disentanglement at higher frequencies and the other is due to backbone relaxation at lower frequencies. As a consequence of having entangled branches, the maximum value of Q_0 corresponds to the backbone relaxation ($Q_{0,b}$). It is much lower than that of comb PS with unentangled branches (C622). When two comb PSs with entangled branches (C632 and C642) are compared, as the entangled branch chain length becomes longer, the $Q_{0,b}$ becomes lower and the $Q_0(\omega)$ becomes narrower. The Q_0 coefficient reflects the relaxation process of disentanglement of polymer chain, including reptation, contour fluctuation, and constraint release, very well for the monodisperse linear PS and comb PS.

For the monodisperse linear PS, the Q shows a reduction as the strain amplitude increases at various fixed frequency ($Q(\gamma_0)$ decreasing). Conversely, for the comb PS with entangled branches, the Q increases as the strain amplitude increases at specific frequencies ($Q(\gamma_0)$ increasing). This nonlinear coefficient Q behavior is related to the polymer topology; therefore, Q as a function of strain amplitude will be investigated toward long chain branching of commercial branched polymers. However, we still do not fully understand the underlying physics of $Q(\gamma_0)$ behavior such as the increase in $Q(\gamma_0)$ as a function of the strain amplitude. Therefore, further theoretical and experimental studies are needed to understand the Q behavior as a function of the strain amplitude of entangled polymer with different topology. From these results, it is evident that the

nonlinear coefficient (Q) from FT-rheology under oscillatory shear is a new and very promising coefficient for quantifying the inherent mechanical nonlinearity, for example, between linear polymer and polymer with different topology, especially branched chains. From this first systematic investigation, we determine a relationship between the relaxation process of polymer chains and the nonlinearity from FT-rheology.

Furthermore, it is very important that within the concept of the Q coefficient and the high sensitivity of FT-rheology a linear regime is only the asymptotic approximation for vanishing nonlinearities. This can lead to the argument that linear response is achieved for only vanishing deformations and thus never for any real experiment. Nevertheless, it is commonly accepted that the linear response can very accurately describe the mechanical response. To overcome this conceptional problem, we might define the linear regime in oscillatory shear test (SAOS) as the regime in which the experimental response can be approximated by, for example, 99.5% of linear rheological properties (G' or G''), or alternatively, nonlinearity $I_{3/1} < 0.5\%$ ($\sim 5 \times 10^{-3}$) from FT-rheology.

Despite this study being focused on determining the Q coefficient for polymer melts, the concept of the Q coefficient can be widely applied for any other complex fluid systems.

Acknowledgment. K.H. thanks the Max-Planck Society and the Technical University of Darmstadt for financial support and Dimitris Vlassopoulos (University of Crete) for supplying the comb PS series. We thank Prof. G. McKinley (MIT) for a discussion about the limits of the linear response theory.

Appendix A

The shear stress under nonlinear oscillatory shear from FT-rheology[9] is described as follows

$$\begin{aligned}\sigma(t) &= \sigma_1 \sin(\omega t + \delta_1) + \sigma_3 \sin(3\omega t + \delta_3) + \cdots \\ &= \sigma_1 \cos\delta_1 \sin\omega t + \sigma_1 \sin\delta_1 \cos\omega t + \sigma_3 \cos\delta_3 \sin 3\omega t + \\ &\qquad \sigma_3 \sin\delta_3 \cos 3\omega t + \cdots \end{aligned} \tag{A1}$$

From the above equation, we can calculate the relative third intensity from FT-rheology as follows

$$\frac{I_3}{I_1} = \frac{\sigma_3}{\sigma_1} = \frac{\sqrt{(\sigma_3 \cos\delta_3)^2 + (\sigma_3 \sin\delta_3)^2}}{\sqrt{(\sigma_1 \cos\delta_1)^2 + (\sigma_1 \sin\delta_1)^2}} \tag{A2}$$

The shear stress under nonlinear oscillatory shear from Pearson and Rochefort[33] is described as follows

$$\begin{aligned}\text{1st nonlinear term} &= [G'_{11}\gamma_0 + G'_{31}\gamma_0^3 + O(\gamma_0^5) + \cdots] \sin\omega t + \\ &\qquad [G''_{11}\gamma_0 + G''_{31}\gamma_0^3 + O(\gamma_0^5) + \cdots] \cos\omega t \end{aligned} \tag{A3}$$

$$\begin{aligned}\text{3rd nonlinear term} &= [G'_{33}\gamma_0^3 + G'_{53}\gamma_0^5 + O(\gamma_0^7) + \cdots] \sin 3\omega t + \\ &\qquad [G''_{33}\gamma_0^3 + G''_{53}\gamma_0^5 + O(\gamma_0^7) + \cdots] \cos 3\omega t \end{aligned} \tag{A4}$$

These two definitions describethe same nonlinear phenomena; therefore, we can calculate the Q coefficient by inserting eqs A3 and A4 into A2

$$\begin{aligned} Q &= \frac{I_3}{I_1}\frac{1}{\gamma_0^2} \\ &= \frac{\sqrt{(G'_{33}\gamma_0^3 + G'_{53}\gamma_0^5 + \cdots)^2 + (G''_{33}\gamma_0^3 + G''_{53}\gamma_0^5 + \cdots)^2}}{\sqrt{(G'_{11}\gamma_0 + G'_{31}\gamma_0^3 + \cdots)^2 + (G''_{11}\gamma_0 + G''_{31}\gamma_0^3 + \cdots)^2}}\frac{1}{\gamma_0^2} \\ &= \frac{\sqrt{{G'_{33}}^2\gamma_0^6 + {G''_{33}}^2\gamma_0^6 + O(\gamma_0^8)\cdots}}{\sqrt{{G'_{11}}^2\gamma_0^2 + {G''_{11}}^2\gamma_0^2 + O(\gamma_0^4)\cdots}}\frac{1}{\gamma_0^2} \\ &= \frac{\sqrt{{G'_{33}}^2 + {G''_{33}}^2 + O(\gamma_0^2)\cdots}}{\sqrt{{G'_{11}}^2 + {G''_{11}}^2 + O(\gamma_0^2)\cdots}} \end{aligned} \tag{A5}$$

At low-strain amplitude limits of Q coefficient, we can calculate the zero-strain nonlinearity, $Q_0(\omega)$

$$\begin{aligned} Q_0(\omega) &= \lim_{\gamma_0\to 0}\frac{I_3}{I_1}\frac{1}{\gamma_0^2} = \lim_{\gamma_0\to 0}\frac{\sqrt{{G'_{33}}^2\gamma_0^6 + {G''_{33}}^2\gamma_0^6 + O(\gamma_0^8) + \cdots}}{\sqrt{{G'_{11}}^2\gamma_0^2 + {G''_{11}}^2\gamma_0^2 + O(\gamma_0^4) + \cdots}}\frac{1}{\gamma_0^2} \\ &= \lim_{\gamma_0\to 0}\frac{\sqrt{{G'_{33}}^2 + {G''_{33}}^2 + \cdots}}{\sqrt{{G'_{11}}^2 + {G''_{11}}^2 + \cdots}}\frac{\gamma_0^3}{\gamma_0}\frac{1}{\gamma_0^2} \\ &= \frac{\sqrt{G'_{33}(\omega)^2 + G''_{33}(\omega)^2}}{\sqrt{G'_{11}(\omega)^2 + G''_{11}(\omega)^2}} = \frac{|G^*_{33}(\omega)|}{|G^*_{11}(\omega)|} \end{aligned} \tag{A6}$$

From eq A6, $Q_0(\omega)$ can directly connect with the definition of Pearson and Rochefort and the $Q_0(\omega)$ mean normalized third nonlinear complex modulus (3rd nonlinear term) divided by the linear complex modulus (1st nonlinear term). These definitions can generally be used for any complex fluid.

Appendix B

Pearson and Rochefort calculated the nonlinear coefficients using the Doi−Edwards model[33] for entangled polymer

$$G'_{11}(\omega) = \frac{3}{5}\frac{\rho kT}{N_e}\sum_{p,odd}^{\infty}\frac{8}{\pi^2 p^2}\frac{\omega^2\tau_d^2}{p^4 + \omega^2\tau_d^2} \tag{B1}$$

$$G''_{11}(\omega) = \frac{3}{5}\frac{\rho kT}{N_e}\sum_{p,\mathrm{odd}}^{\infty}\frac{8}{\pi^2 p^2}\frac{\omega\tau_d}{p^4 + \omega^2\tau_d^2} \tag{B2}$$

$$\begin{aligned} G'_{33}(\omega) = \frac{3}{28}\frac{\rho kT}{N_e}\sum_{p,\mathrm{odd}}^{\infty}\frac{8}{\pi^2 p^2}\Bigg(&\frac{\omega^2\tau_d^2}{p^4 + \omega^2\tau_d^2} - \frac{4\omega^2\tau_d^2}{p^4 + 4\omega^2\tau_d^2} + \\ &\frac{3\omega^2\tau_d^2}{p^4 + 9\omega^2\tau_d^2}\Bigg) \end{aligned} \tag{B3}$$

$$\begin{aligned} G''_{33}(\omega) = \frac{3}{28}\frac{\rho kT}{N_e}\sum_{p,\mathrm{odd}}^{\infty}\frac{8}{\pi^2}\Bigg(&\frac{\omega\tau_d}{p^4 + \omega^2\tau_d^2} - \frac{2\omega\tau_d}{p^4 + 4\omega^2\tau_d^2} + \\ &\frac{\omega\tau_d}{p^4 + 9\omega^2\tau_d^2}\Bigg) \end{aligned} \tag{B4}$$

The low-frequency limits of the dynamic moduli are

$$G'_{11}(\omega) \cong \frac{3}{5}\frac{\rho kT}{N_e}\sum_{p,odd}^{\infty}\frac{8}{\pi^2}\frac{\omega^2\tau_d^2}{p^6} \tag{B5}$$

$$G''_{11}(\omega) \cong \frac{3}{5}\frac{\rho kT}{N_e}\sum_{p,\mathrm{odd}}^{\infty}\frac{8}{\pi^2}\frac{\omega\tau_d}{p^4} \tag{B6}$$

$$G'_{33}(\omega) \cong \frac{3}{28}\frac{\rho kT}{N_e}\sum_{p,\text{odd}}^{\infty}\frac{8}{\pi^2}\frac{-12\omega^4\tau_d^4}{p^{10}} \tag{B7}$$

$$G''_{33}(\omega) \cong \frac{3}{28}\frac{\rho kT}{N_e}\sum_{p,\text{odd}}^{\infty}\frac{8}{\pi^2}\frac{-2\omega^3\tau_d^3}{p^{8}} \tag{B8}$$

$$\lim_{\omega\to 0} Q_0(\omega) = \lim_{\omega\to 0}\frac{\sqrt{{G'_{33}}^2+{G''_{33}}^2}}{\sqrt{{G'_{11}}^2+{G''_{11}}^2}} \propto \lim_{\omega\to 0}\frac{\sqrt{\omega^6+\omega^8}}{\sqrt{\omega^4+\omega^2}} \propto \lim_{\omega\to 0}\frac{\omega^3}{\omega} \propto \omega^2 \tag{B9}$$

Therefore, a quadratic scaling ($Q_0 \propto \omega^2$) at the low-frequency limit using the Doi−Edwards model from Pearson and Rochefort can be assumed for $Q_0(\omega)$.

References and Notes

(1) Yosick, J. A.; Giacomin, A. J.; Moldenaers, P. *J. Non-Newtonian Fluid Mech.* **1997**, *70*, 103.
(2) Dealy, J. M.; Wissbrun K. F. *Melt Rheology and Its Role in Plastics Processing: Theory and Applications*; VNR: New York, 1990.
(3) Hyun, K.; Kim, S. H.; Ahn, K. H.; Lee, S. J. *J. Non-Newtonian Fluid Mech.* **2002**, *107*, 51.
(4) Hamley, I. W.; Pople, J. A.; Booth, C.; Derici, L.; Imperor-Clerc, M.; Davidson, P. *Phys. Rev. E* **1998**, *58*, 7620.
(5) Hyun, K.; Nam, J. G.; Wilhelm, M.; Ahn, K. H.; Lee, S. J. *Korea-Australia Rheol. J.* **2003**, *15*, 97.
(6) Sugimoto, M.; Suzuki, Y.; Hyun, K.; Ahn, K. H.; Ushioda, T.; Nishioka, A.; Taniguchi, T.; Koyama, K. *Rheol. Acta* **2006**, *46*, 33.
(7) Ewoldt, R. H.; Clasen, C.; Hosei, A. E.; McKinley, G. H. *Soft Matter* **2007**, *3*, 634.
(8) Wilhelm, M.; Reinheimer, P.; Ortseifer, M. *Rheol. Acta* **1999**, *38*, 349.
(9) Wilhelm, M. *Macromol. Mater. Eng.* **2002**, *287*, 83.
(10) Cho, K. S.; Hyun, K.; Ahn, K. H.; Lee, S. J. *J. Rheol.* **2005**, *49*, 747.
(11) Carotenuto, C.; Sioula, S.; Grosso, M.; Maffettone, P. L. *Macromolecules* **2008**, *41*, 4492.
(12) Klein, C. O.; Spiess, H. W.; Calin, A.; Balan, C.; Wilhelm, M. *Macromolecules* **2007**, *40*, 4250.
(13) Neidhöfer, T.; Sioula, S.; Hadjichristidis, N.; Wilhelm, M. *Macromol. Rapid Commun.* **2004**, *25*, 1921.
(14) Fleury, G.; Schlatter, G.; Muller, R. *Rheol. Acta* **2004**, *44*, 174.
(15) Schlatter, G.; Fleury, G.; Muller, R. *Macromolecules* **2005**, *38*, 6492.
(16) Vittorias, I.; Parkinson, M.; Klimke, K.; Debbaut, B.; Wilhelm, M. *Rheol. Acta* **2007**, *46*, 321.
(17) Hyun, K.; Ahn, K. H.; Lee, S. J.; Sugimoto, M.; Koyama, K. *Rheol. Acta* **2006**, *46*, 123.
(18) Hyun, K.; Baik, E. S.; Ahn, K. H.; Lee, S. J.; Sugimoto, M.; Koyama, K. *J. Rheol.* **2007**, *51*, 1319.
(19) Williams, D. J. *Angew. Chem., Int. Ed. Engl.* **1984**, *23*, 690.
(20) Roovers, J.; Graessley, W. W. *Macromolecules* **1981**, *14*, 766.
(21) Roovers, J.; Toporowski, P. M. *Macromolecules* **1987**, *20*, 2300.
(22) Ferry, J. D. *Viscoelastic Properties of Polymers*; Wiley: New York, 1980.
(23) Kapnistos, M.; Vlassopoulos, D.; Roovers, J.; Leal, L. G. *Macromolecules* **2005**, *38*, 7852.
(24) van Dusschoten, D.; Wilhelm, M. *Rheol. Acta* **2001**, *40*, 395.
(25) McLeish, T. C. B. *Europhys. Lett.* **1988**, *6*, 511.
(26) McLeish, T. C. B. *Adv. Phys.* **2002**, *51*, 1379.
(27) McLeish, T. C. B.; Milner, S. T. *Adv. Polym. Sci.* **1999**, *199*, 195.
(28) Milner, S. T.; McLeish, T. C. B. *Phys. Rev. Lett.* **1998**, *81*, 725.
(29) Nam, J. G.; Hyun, K.; Ahn, K. H.; Lee, S. J. *J. Non-Newtonian Fluid Mech.* **2008**, *150*, 1.
(30) Larson, R. G. *The Structure and Rheology of Complex Fluids*; Oxford University Press: New York, 1999.
(31) Chen, Y. L.; Larson, R. G.; Patel, S. S. *Rheol. Acta* **1994**, *33*, 243.
(32) van Dusschoten, D.; Wilhelm, M.; Spiess, H. W. *J. Rheol.* **2001**, *45*, 1319.
(33) Pearson, D. S.; Rochefort, W. E. *J. Polym. Sci., Polym. Phys. Ed.* **1982**, *20*, 83.
(34) Watanabe, H. *Macromol. Rapid Commun.* **2001**, *22*, 127.

MA8017266